ELECTRON IMAGING TECHNIQUES

R.H. WADE

Section de Physique du Solide
Département de Recherche Fondamentale
Centre d'Etudes Nucléaires de Grenoble
85 X, 38041 Grenoble Cédex, France

1. INTRODUCTION

Our aim is to give an introductory description of the electron microscope suitable for those having no acquaintance with this field. We will describe how the instrument is used to obtain the maximum possible amount of information about different types of specimen with particular attention to biological specimens.

There are so many types of electron beam instruments that it will not be possible to describe them all. Particular attention will be paid to the high resolution instruments which are still being actively developped because of their importance for ultrastructural research.

It is well known that any optical instrument has an ultimate resolution limit (r) of the form

$$r = \lambda/\alpha$$

depending both on the angular aperture of the system α and on the radiation wavelength λ. The de Broglie wavelength associated with an electron of mass m moving with velocity v is

$$\lambda = h/mv$$

where h is Planck's constant. By equating the kinetic and potential energy we obtain the electron wavelength in terms of the accelerating potential,

$$\lambda_e = (150/V)^{1/2}\ \text{Å}, \text{ where } 1\ \text{Å} = 10^{-8}\ \text{cm}, \text{ is in volts.}$$

The wavelength of an electron accelerated through 100 keV is $\lambda_e \simeq 4 \times 10^{-10}$ cm which is well below atomic dimensions so a dramatic improvement in resolution is possible compared with photons of wavelength $\lambda \simeq 5 \times 10^{-5}$ cm. The best electron lenses so far devised have aberrations which limit of the resolution to $\sim 100\ \lambda_e$. These lenses consist of many turns of copper wire round a soft iron core in the gap of which specially shaped soft-iron pole pieces constitute the lens itself.

2. MAGNETIC LENSES AND THEIR ABERRATIONS

The quality of the lens depends on the pole piece geometry. The most important parameters being the spacing between the upper and lower pole pieces and the diameters of the bore of the two parts. Electrons travelling at a small angle to the optical axis are focussed by the magnetic field between the pole pieces. In the thin lens approximation the focal length (f) of the lens is given by :

$$\frac{1}{f} = \frac{1.75}{V} \int H_z^2 \, dz \quad ; \quad f = \text{const} \quad V/I^2$$

where V is the electron energy in volts and H_z is the axial component of the field in amp/m , f is in cm, I is the excitation current of the lens [1].

Of the third order aberrations for a magnetic lens the spherical aberration does not vanish on the optical axis [2,3]. Since the focal length depends on the square of the field all electron lenses are positive so there is no way of correcting this defect in a rotationally symmetric, charge free system [4].

The rays incident on the lens at an angle θ are deflected through an angle $C_s\theta^3$; these rays are focussed nearer to the lens than the axial rays which form the Gaussian image (C_s the spherical aberration constant is in the range 0.07 - 0.15 cm for the best magnetic lenses). In fact, a caustic surface is associated with this aberration. It can be shown that the associated disc of least confusion has a diameter of $C_s\theta_m^3$ and is situated at $3\,C_s\,\theta_m^3/4$ in front of the Gaussian image plane [5]. On this arguement the resolution limit is reached when the lens aperture is such that the Airy disc associated with the diffraction by this aperture is equal to the disc of least confusion due to spherical aberration. To within multiplicative constants this gives $C_s\,\theta^3 = \lambda/\theta$ which yields a resolution $r = (C_s\,\lambda^3)^{1/4}$.

The wave aberration associated with the lens is $W(\theta) = 2\pi/\lambda\ (-z\theta^2/2 + C_s\theta^4/4)$ where z is the defocussing distance [6-9]. This phase term is stationary for $\theta = 0$ or $\sqrt{C_s/z}$. It can be shown that for maximum phase contrast $W(\theta) = \pi/2$ whence we find that for a defocus $z = (C_s\,\lambda)^{1/2}$ (Scherzer defocus) the resolution is given by $r = (C_s\,\lambda^3)^{1/4}$ in agreement with the semi-geometrical arguement above. In fact the resolution is more correctly discussed in terms of contrast transfer theory [6-9] which shows that by varying the defocus z we can "tune-in" to different spatial frequency bands.

The electrical supplies of the microscope are never perfectly stable. If δV is the fluctuation of the high tension supply V and δI that of the lens current we find a varying defocus $\delta f = C_c\,\{\frac{\delta V}{V} - 2\,\frac{\delta I}{I}\}$ where the constant C_c is called the chromatic aberration constant of the lens, and is in the range 0.1 to 0.2 cm. The beam itself has an energy spread equivalent to the voltage fluctuation ΔV part of which is thermal and part due to space charge - the Boersch effect [10 - 12]. Since all these

fluctuations are independant it seems reasonable to take the RMS value as the defocus fluctuation :

$$\delta z = C_c \{ (\frac{\delta V}{V})^2 + 2 (\frac{\delta I}{I})^2 + (\frac{\Delta V}{V})^2 \}^{1/2}$$

The effect of this fluctuating defocus is to limit the resolution. It can be shown quite generally that for parallel illumination the image of an object of period d is identical in planes separated by defocus increments $\delta z = 2 d^2/\lambda$ and that the contrast reverses at half this distance. From this equality we find that in the presence of a defocus fluctuation δz the resolvable periodic components (r) in the object must satisfy the inequality $r \geq (\lambda \delta z)^{1/2}$.

In the contrast transfer theory the effect of this chromatic fluctuation is described by an envelope function which attenuates the higher spatial frequencies in the object giving a cut-off frequency in agreement with the above inequality to within a constant factor.

Astigmatism results from departure from exact cylindrical symmetry in the lens. Its effect is that different directions in the object do not fall in focus in the same plane. It is as if the lens has different focal lengths in two perpendicular planes. This defect is easily corrected by using compensating coils built into the lens regions.

3. TRANSMISSION ELECTRON MICROSCOPE : CTEM

The strong absorbtion of electrons by matter requires that the electron beam runs within a vacuum enclosure. The electrons emitted from a heated tungsten filament are accelerated to the operating voltage by the potential difference applied between the filament and an anode which is at the same potential as the microscope column. For obvious reasons, the filament is at a negative potential and the microscope column at earth ! An automatically biased triode system is usual. The bias voltage determines the total emission current. The brightness of such a source is $10^4 - 10^5$ A/cm^2/sterad. The optics of the triode produces a cross-over region between the filament and the anode. This minimum cross-section acts as the effective source and has a diameter of about 10^{-2} cm, [1].

A double condenser lens system enables the beam to be focussed at the specimen plane with varying cross-over sizes and beam currents. This enables the illuminated area to be limited to the field of view. The first condenser lens is strong and the second lens projects the highly demagnified image onto the specimen. The minimum spot diameter at the specimen is 2 µm. The use of the second lens allows an adequate working space between the condenser system and the object. Since the brightness is constant within an optical system the current density in the spot illuminating the

object is $j_o = j_s (\phi_o/\phi_s)^2$ and depends on the solid angles ϕ_o and ϕ_s subtended by the condenser aperture at the object and the source respectively. Typically j_o is of the order 1 amp/cm^2 or less,[1, 2, 13].

The specimen is situated just above the objective lens of the microscope. In practice it may be within the magnetic field of this lens. The pre-field can be considered as part of the condenser system. The electron beam is scattered by the specimen with an angular distribution which can be visualised in the back focal plane of the objective lens, this is the Fraunhofer diffraction image of the object. Apertures placed in this plane can delimit which part of the scattering distribution contributes to the image (spatial frequency filtering). The focal length of the objective lens is in the range 0.1 - 0.2 cm so that a scattering angle of 2×10^{-2} rad will correspond to a diffraction spot about 30 µm off the axial unscattered beam. Objective aperture sizes used to exclude these scattered beams will be in the range 10 - 100 µm diameter.

The objective lens produces an image magnified in the range 10 - 50 x. This image is further magnified by a projector lens system of two or three lenses to produce a final image whose magnification can be varied over a wide range from below 5,000 up to 500,000 or more. The focal length of the lens below the objective lens can be varied so that the final image plane is conjugate either to the object or to the back focal plane.

The final image is viewed on a fine grain fluorescent screen which has an efficiency of about 25 % for the conversion of electrons to photons. This efficiency increases with accelerating voltage up to 100 keV and then falls off. Only about 2×10^{-4} of all the emitted light is collected by the eye. The resolving power of the screen is of the order 100 µm. The screen is viewed through a lead-glass port offering X-ray protection. Binocular viewing permits fine focussing. Images are recorded on photographic plates or film stored in a holder below the viewing screen.

4. SCANNING TRANSMISSION ELECTRON MICROSCOPE : STEM [14]

The electron source is a field emission electron gun consisting of a pointed tungsten filament and an extraction electrode. The filament tip is roughly hemispherical with a radius R $\sim$ 500 Å. When the extraction electrode is held at a few kilovolts the field generated in the region of the tip is of the order of 1 volt/Å. This causes electrons to be drawn from the tip by the tunnel effect. These electrons are accelerated up to the working voltage 20 - 100 keV in one or several stages. Since the electrons are emitted radially from the tip the apparent source size r is much smaller than the tip, $r = R(V_T/V)^{1/2}$, where V_T is the energy spread of the emitted

electrons (V_T < 0.5 eV) and V the accelerating potential (V ∿ 1 keV). This gives an apparent source radius of 10 Å.

The gun operates as a stable source in the absence of adsorped layers and therefore requires a very high vacuum in the region of the tip. For this reason the gun chamber is usually differentially pumped to better than 10^{-10} torr. This type of gun has a brightness of the order 10^8 amp/cm^2/sterad.

The image of the source produced by the gun optics is about 100 Å in diameter. The simplest scanning microscopes consist of the gun and an "objective" lens ; an additional condenser lens is sometimes added. In either case the spot size δ at the specimen is about 5 Å and is essentially spherical aberration limited, $\delta \simeq 0.7(C_s\lambda^3)^{1/4}$.

Since the energy spread associated with field emission is small (< .25 volts) the chromatic aberration of the objective lens does not limit the spot size. Recent results indicate that at high beam currents the energy spread may become much larger [32]. A beam current of about 10^{-8} amps can be obtained in a spot size of 10 Å in a commercially available instrument.

The specimen is situated after the objective lens. The illumination spot is scanned across the specimen in a raster generated by sets of coils placed between the source and the objective lens. Detectors placed after the specimen pick-up the scattered electrons and a cathode ray tube scanned synchronously is modulated according to the electron current. The magnification depends only on the size of the scanning raster at the specimen. There are no lenses after the specimen. This makes it easy to fit an energy analyser. The function of the detectors is described in the section on contrast mechanisms.

5. SPECIMENS

The specimens examined in metallurgy and solid state physics are prepared in a variety of ways. They must be thin which in practice can mean in the thickness range from a few tens to several thousand Å units. The final thinning operation may consist of electrolytic or chemical polishing, ion bombardement, cleavage, grinding and vacuum deposition. The aim is to obtain the largest possible electron transparent area. The specimens may be self supporting or mounted on copper grids, [13].

Biological materials are dehydrated by the vacuum within the microscope and are destroyed by electron irradiation. In addition most biological specimens have low contrast in bright field electron microscopy. Some materials are embedded in resins and sliced-up on an ultramicrotome whilst others can be placed on a thin carbon support. In both cases negative stains of heavy metal salts are used to preserve and

enhance the contrast from structural irregularities. The stain engulfs the material and forms a glass-like mould. The best resolution of material so treated is found to be around 20 Å and is related to the grain of the staining material.

6. CONTRAST MECHANISMS

6.1. Scattering

6.1 (a) - Elastic scattering. The atomic scattering factor has the form :

$$f(\theta) = \frac{m_o e^2}{2h^2} \left(\frac{\lambda}{\sin \theta}\right)^2 (Z - f_x)$$

where $m_o e^2/2h^2 = 2.38 \times 10^6$ cm^{-1} [15]. The first term in the bracket is due to Rutherford scattering from the nucleus and the second term, the atomic scattering factor for X-rays, is due to scattering from the electron cloud. The differential scattering cross section is directly related to $f(\theta)$, $d\sigma_e(\theta)/d\Omega = f^2(\theta)$. The variation of $d\sigma_e/d\Omega$ as a function of θ is schematised in figure 1 for 100 keV electrons. The figure is equivalent to a radial section across the diffraction image obtained in the back focal plane of the objective lens. The total number of electrons scattered through an angle θ is obtained by integration over an annulus of radius proportional to θ. Since the cone of the incident radiation has typically an angle of 10^{-3} rad, it is seen that most electrons are scattered outside the cone of the transmitted beam. The total scattering cross section σ_e found by integrating $f^2(\theta)$ over all scattering angles is $\sigma_e \propto Z^{4/3}$ using an exponentially screened Coulomb atomic potential distribution. Experimentally σ_e would be obtained by collecting all the elastically scattered electrons.

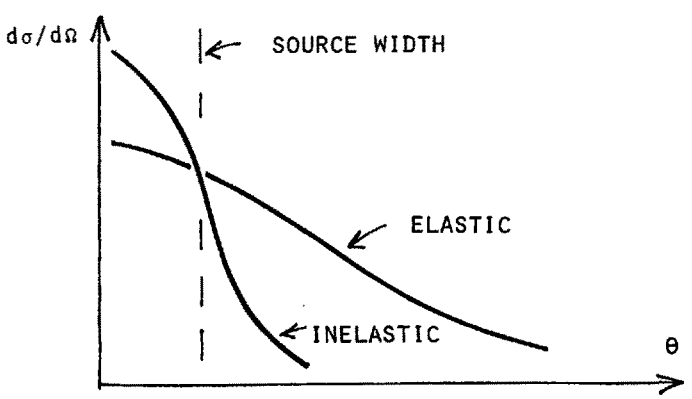

Figure 1 - The angular dependence of the elastic and inelastic differential scattering cross sections compared to the source width.

6.1 (b) - Inelastic scattering . There are many processes by which energy is transferred from the electron beam to the irradiated material [16]. For the light atoms present in biological material the probability of an inelastic scattering process is about twice that of an elastic one. The differential scattering cross section $d\sigma_i/d\Omega$ is given by

$$\frac{d\sigma_i}{d\Omega} = \text{const} \frac{1}{\theta^2 + \theta_E^2}$$

θ is the scattering angle and the screening angle $\theta_E = \Delta E/2\ E_o$ where ΔE is the energy loss, typically in the range 1 - 40 eV, and E_o is the incident electron energy [16]. This distribution is sharply peaked in the forward direction for angles less than θ_E, ie $\theta_{max} < 10^{-3}$ rad. The total inelastic cross section varies according to the atomic model. In the Lenz theory [17] using a Thomas-Fermi model and for single electron excitation $\sigma_i \propto Z^{1/3}$.

The essentiel point is that the beam transmitted through a thin specimen consists of three parts. The unscattered beam N_o ; the elastically scattered component N_e ; the inelastically scattered component N_i.

6.2. Imaging

6.2 (a) - CTEM : A perfect lens collecting all the scattered electrons would form an image directly representing the square modulus of the electron wave function at the exit face of the specimen. In the absence of electron absorbtion the image so formed would show no contrast. Image contrast can be generated either by introducing apertures into the back focal plane of the objective lens in order to select a particular angular component of the overall scattering distribution (Fraunhofer diffraction amplitude) or by using the objective lens defocus as a means of introducing phase shifts between the scattered and unscattered components.

1) Diffraction contrast : a small aperture selects the electrons corresponding to essentially one scattering angle. In the bright field method the aperture selects the unscattered beam. The image will show modulations of intensity depending on the local scattering at the specimen. The resolution, depending on the aperture size, is relatively low. The method is commonly used in work on single crystals. If the aperture is placed over a scattered beam a dark field image is produced. A great deal of information concerning the nature of crystal defects can be obtained by this method [13].

2) Bright field interference contrast : in this case the scattered and unscattered beams are allowed to pass into the image where they interfere. When $N_o >> N_e$ the image contrast is proportional to the object exit surface wave function. For lattice

plane images the incident beam can be tilted so the unscattered and scattered waves make equal angles with the optical axis in which case the image is aberration free. Images combining many diffracted beams have been successfully exploited in the study of complex oxide crystals. In this case the lens aberrations and finite source size must be taken into account. This is usually done by a comparison of experimental and digitally generated images. The agreement can be quite impressive, a simple account is given in [18].

The method can also be applied to crystals of biological interest exposed under low dose conditions in order to minimise the radiation damage. The images consist of a periodic signal with a strong noise superposed. Digital treatment of the images enables the periodic component to be separated from the noise and since both the amplitudes and phases of the Fourier components are obtained a Fourier synthesis of the crystal structure can be made [19-21]. Image processing can also be carried out optically [22, 23].

3) Dark field : the image is formed with the scattered electrons only. The idea being that since it is only these electrons which carry information about the object they alone should be retained in preference to the unscattered electrons. In one method a central stop is used. Although difficult to realise experimentally, this gives a good collection efficiency for the elastically scattered electrons whilst a good deal of the inelastic scattering can be cut out by the stop along with the unscattered beam. Another method uses a circular aperture whilst the incident beam is tilted. This method gives less efficient electron collection and it is rather more difficult to take account of the effect of lens aberrations. Images of low molecular weight proteins may yield valuable high resolution (< 10 Å) information after some image averaging [24].

6.2 (b) STEM : There are no lenses after the object so the detection takes place essentially in the far-field or Fraunhofer diffraction region. Use is made of the different angular distributions of the elastic and inelastic electrons to separate all three beam components. An annular aperture collects the elastically scattered electrons, the unscattered and inelastic electrons pass through the central hole and are separated by an energy filter. The three signals can be detected simultaneously.

1. Dark field : The signal N_e (or N_e/N_o) corresponds to the dark field image with an extremely good efficiency since the annular aperture corresponds to a very large collecting angle for the elastic electrons. The signal is approximately proportional to σ_e

2. Z contrast : The ratio $N_e/N_i \approx \sigma_e/\sigma_i$ gives a signal which is proportional to Z or to some power of Z depending on the form taken for the scattering potential. This method has no equivalent in the CTEM and has been greatly exploited by Crewe and his collaborators for the visualisation of heavy atoms [14].

3. Bright field : The detector angle must be very small and the illumination angle large. It is then possible to observe phase contrast and lattice images as in bright field CTEM [33]. The method compares unfavourably to the CTEM as far as the object irradiation is concerned.

7. RECIPROCITY

It is found experimentally that STEM images can be similar to CTEM images. Examples are Fresnel fringes, phase contrast, lattice images. From the description of the two instruments it is not at all abvious that the two instruments give similar results since the CTEM involves detection in a plane conjugate to the object whilst the STEM detection plane appears roughly conjugate to the illumination aperture.

However if we consider the two systems as they are represented in figure 2 we see that, in STEM, electrons from a point A of the source are focussed on the specimen and the intensity detected at B far below the specimen. In CTEM electrons from a distant point B' of the source are scattered by the specimen and focussed by the lens to the image point A'.

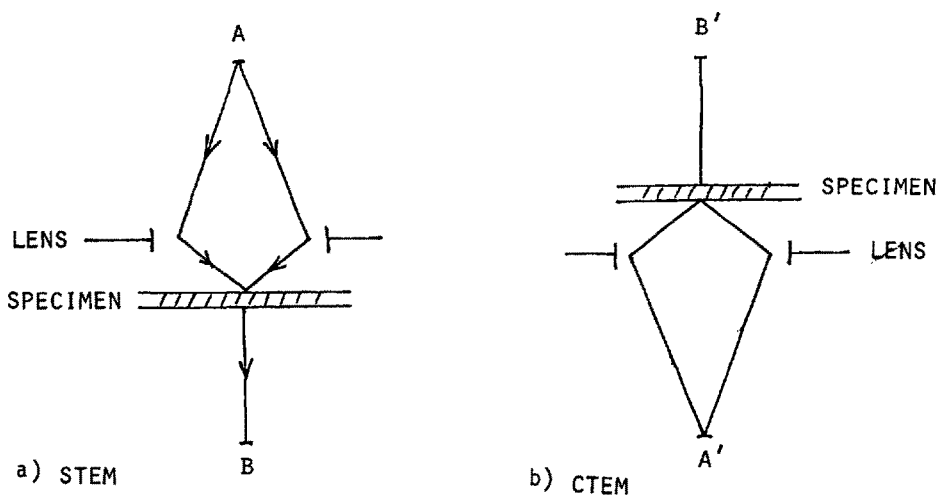

Figure 2 - The imaging process in STEM and CTEM are schematised in (a) and (b) respectively. Inversion of the ray directions in one diagram gives the other so the two methods are related by reciprocity.

The Helholtz reciprocity theorem would suggest that in fig. 2(a) the point source A will produce the same effect at B as a point source of equal intensity at B would produce at A. Comparison of fig. 2(a) and (b) shows that (b) is just an inversion of (a), provided the specimen is inverted. The two microscopes are therefore equivalent ; in STEM the detector size plays the same resolution limiting role for phase contrast images as does the source in CTEM [25, 26]. However the two microscopes are not equivalent as far as radiation dose is concerned.

8. RESOLUTION LIMITS

That part of the image intensity distribution directly related to the scattering due to the object represents the useful signal. The rest is noise and includes :

1) inelastic electrons which contribute essentially a low contrast low resolution background.

2) the elastic image of the specimen substrate, for example the phase contrast image of the carbon support used for biological materials.

3) electrons scattered through large angles whose contribution to the image is blurred out by the enveloppe functions associated with a finite source size and chromatic defocus fluctuations.

4) shot noise which depends on the number of electrons detected within a "resolution cell" and so on the electron dose at the specimen.

A useful relationship which indicates the number of quanta (n/unit area) necessary to image an object of contrast c at a resolution d is the Rose expression

$$n \geqslant (t/cd)^2,$$

where the threshold signal to noise ratio t will typically have a value of around 5 [27].

A thermal source imaged onto the specimen plane by the condenser lenses can easily give a radiation dose of 60 el/$\mathring{A}^2$/sec. For a total magnification of 4×10^4 an intensity at the fluorescent screen equivalent to about 2 el/$\mathring{A}^2$/sec at the object is required to allow visual observation and focussing. At the same magnification a photograph of unit average density requires a dose of $\sim$ 1 el/$\mathring{A}^2$ at the object.

Since biological material is destroyed by doses in the range .05- several el/$\mathring{A}^2$ [28, 29] meaningful observations on biological material require very low total electron doses. The Rose expression then shows that the attainable resolution is severely limited. The resolution can be improved by averaging over a number of identical

objects. This can be achieved by either using two dimensional crystal arrays [20], or adding images of isolated molecules [30]. Other possibilities are :

1) to increase the contrast using the dark field method [24]. The doses used destroy the structure but the remaining "skeleton" seems to be closely related to the original structure in the case of low molecular weight proteins ($\sim$ 1000 daltons). Image averaging is also required. Equivalent results should be attainable by subtracting the background intensity from bright field images.

2) Recent results suggest that the radiation resistance may be dramatically improved if the specimens are cooled to liquid helium temperatures [31]. If these results are confirmed a dramatic breakthrough in biological structure investigation by electron microscopy will be possible.

References

[1] M.E. HAINE, The Electron Microscope, Spon Ltd, (1961).
[2] C.E. HALL, Introduction to Electron Microscopy, Mc Graw Hill, (1953).
[3] M. BORN and E. WOLF, Principles of Optics, Permagon Press (1964).
[4] O. SCHERZER, Z. Physik 101, 593 (1936).
[5] D. GABOR, Proc. Roy. Soc. A 197, 454 (1949).
[6] O. SCHERZER, J. Appl. Physics, 20, 20, (1949).
[7] K.J. HANSSEN, in Advances in Electron and Optical Microscopy, ed. by R. Barer and V.E. Cosslett, vol. 4 pp. 1-84, Academic Press (1971).
[8] P.W. HAWKES, this book.
[9] F.A. LENZ, in Electron Microscopy in Materials Science, ed. by U. Valdré, pp. 541-569, Academic Press (1971).
[10] G. FONTAINE, this book.
[11] H. BOERSCH, Z. Physik 139, 115 (1954).
[12] R.W. DITCHFIELD, M.J. WHELAN, Optik, 48, 163 (1977).
[13] P.B. HIRSCH, A. HOWIE, R.B. NICHOLSON, D.W. PASHLEY, M.J. WHELAN, Electron Microscopy of Thin Crystals, Butterworths (1965).
[14] A.V. CREWE, in Electron Microscopy in Materials Science, ed. by U. Valdré, pp. 162-207, Academic Press (1971).
[15] J. SIVARDIERE, this book.
[16] Ch. COLLIEX, this book.
[17] F.A. LENZ, Z. Naturf. 9a, 185 (1954).
[18] J.M. COWLEY, S. IIJMA, Physics Today, 30, n° 3, 32 (1977).
[19] I.A.M. KUO, R.M. GLAESER, Ultramicroscopy 1, 53 (1975).
[20] P.N.T. UNWIN, R. HENDERSON, J. Mol. Biol. 94, 425 (1975).
[21] D. McLACHLAN, Proc. N.A.S. 44, 948 (1958).
[22] A. KLUG, J.E. BERGER, J. Mol. Biol. 10, 565 (1964).
[23] U. AEBI, P.R. SMITH, J. DUBOCHET, C. HENRY, E.KELLENBERGER, J. Supramol. Structure 1, 498 (1973).
[24] F.P. OTTENSMEYER, D.P. BAZETT-JONES, J. HEWITT, G.B. PRICE, Ultramicroscopy, 3, 303 (1978).
[25] J.M. COWLEY, Appl. Phys. Letters, 15, 58 (1969).
[26] E. ZEITLER, M.G.R. THOMPSON, Optik, 31, 258 (1970).
[27] A. ROSE, Adv. in Electronics, 1, 131 (1948).
[28] K. STENN, G.F. BAHR, J. Ultrastructure Res. 31, 526 (1970).
[29] R.M. GLAESER, J. Ultrastructure Res. 36, 466, (1971).
[30] J. FRANK, W. GOLDFARB, D. EISENBERG, T.S. BAKER, Ultramicroscopy, 3, 283 (1978).
[31] I. DEITRICH, H. FORMANEK, F. FOX, E. KNAPEK, R. WEYL, Nature 277, 380 (1979).
[32] M. TROYON, Optik 52, 401 (1979).
[33] A.J. CRAVEN, C. COLLIEX, J. Microscopie et Spectroscopie Electron. 2, 511 (1977).